Arabian Journal for Science and Engineering (2019) 44:5711–5722
https://doi.org/10.1007/s13369-018-03707-4

RESEARCH ARTICLE - MECHANICAL ENGINEERING

A Novel Heaving Ocean Wave Energy Harvester with a Frequency Tuning Capability

N. V. Viet[1] · A. Carpinteri[2] · Q. Wang[3]

Received: 15 June 2018 / Accepted: 20 December 2018 / Published online: 2 January 2019

Abstract
This study introduces a novel wave energy harvester (WEH) with frequency conversion capability to convert the ocean wave energy to usable electricity based on the piezoelectric effect. The presented WEH is with characteristics of space saving and minimized component quantities and is made of a cylindrical case reciprocally moving with respect to the fixed core shaft attached to identical magnetic bars. The cylindrical case contains four magnetic bar-mass-spring-lever-piezoelectric systems arranged symmetrically each other to the fixed shaft. By this smart design, the WEH is capable of converting the low frequency of ocean waves to a higher excitation frequency of motions on the piezoelectric transducer to harness higher electric power and reduce electrical leakage. A mathematical model of the WEH considering the wave–structure interaction is developed to evaluate the effectiveness of the converter. The simulation results reveal that the occurrence of resonance can lead to an outstanding power output via adjusting the distance between two adjacent magnetic bars. The power output is realized up to 750 W with the converter height and diameter, ocean wave height, and wave period being 1 m, 1 m, 1.5 m and 8 s, respectively.

Keywords Wave energy converter · Piezoelectric technology · Heaving harvester · Ocean wave energy · Frequency conversion · Wave–structure interaction

1 Introduction

The global warming is at an alarming level mostly due to the energy production by burning traditional fossil fuel sources such as oil, gas, and coal that release huge amount of carbon dioxide and other pollutants into the atmosphere. Moreover, traditional fuel is not regenerative, but on higher demand for human development. Hence, energy harvesting from the abundant, sustainable, and harmless energy sources including solar, wind, and ocean waves is indispensable [1]. The energy density of ocean waves is around 2–3 kW/m^2 [2–4] which is the highest compared to that of solar and wind. Besides, the demand on self-power supply for marine devices located on offshore region such as radar, communication devices, desalination devices, marine platforms, and electric charging station located is imperative [5]. Researches on energy harvesting using electrostatic, electromagnetic, and piezoelectric technology to harness energy from ambient vibration sources have achieved fruitful results [6]. Remarkably, the piezoelectric transducer has highest energy density compared to the other two transducers [7,8]. Williams and Yates [7] discovered that the piezoelectric, electromagnetic, electrostatic harvester's power output is proportional to the cube of the excitation frequency. In addition, the piezoelectric transducer has less electric leakage when the excitation frequency of ambient vibration sources is higher than 10 Hz [9]. Gu and Livermore [10] concluded that the piezoelectric energy harvesters with frequency tuning devices are more efficient and effective than those without such tuning devices. The frequency tuning techniques used in harvesting energy from ocean waves are extremely rare [11]. Murray and Rastegar [12] introduced a two-stage electrical energy generator based on the piezoelectric effect, which can convert a low-frequency ocean waves into a much higher frequency mechanical vibrations. The simulation results indicated that the harvester efficiency

✉ N. V. Viet
nguyen.viet@kustar.ac.ae

1 Department of Mechanics, Khalifa University of Science and Technology, PO Box 127788 Abu Dhabi, UAE

2 Department of Structural, Geotechnical and Building Engineering, Politecnico di Torino, Corso Duca degli Abruzzi, Turin, Italy

3 Department of Mechanics and Aerospace Engineering, Southern University of Science and Technology, Shenzhen 518055, Guangdong, People's Republic of China

is highly enhanced. The piezoelectric harvester magnifying the low excitation frequency of vibrational sources other than ocean waves to obtain higher power was also intensively investigated [7,13–17]. Miller et al. [13] presented a Micro-Electro-Mechanical System (MEMS) piezoelectric vibration energy harvester that is able to resonate at low excitation frequencies, matching ambient vibrations found abundantly in buildings. Zhou et al. [14] proposed a magnetically coupled nonlinear piezoelectric energy harvester by altering the angular orientation of its external magnets for enhanced broadband frequency response. Later on, Zhou et al. [16] also introduced an impact-induced method for nonlinear energy harvesters to obtain high-energy orbits over a wide frequency range under low excitation levels. Recently, ocean wave energy harvester based on piezoelectric effect was carried out in studies [18,19]. Results show a nonlinear increase in power output with a rise of excitation frequency.

It is known that ocean waves own powerful mechanical energy, but possess low frequencies. Thus, challenges exist as the currently available transducers can only generate high electric power with high excitation frequencies. High conversion efficiency, simple and easy installation, repair, and maintenance on the harsh environment of offshore region are highly required for newly developed ocean wave converters. In view of these challenges and requirements, a simple and efficient converter using the tension/compression piezoelectric effect to convert a low-wave frequency into higher frequencies of mechanical vibration is presented in this work. To do so, the proposed WEH is designed as a combination of a cylindrical case and a fixed core shaft attached to magnetic bars. The cylindrical case contains four mass, spring, lever, and piezoelectric transducer systems (MLPSs) moving with respect to the fixed core shaft. Each mass of MLPS is attached to a magnetic bar. By this means, the WEH is able to convert the low-frequency ocean waves to the higher excitation frequency of mechanical vibration to increase its energy conversion efficiency. In addition, the WEH is able to utilize the resonant principles to harvest efficiently energy from the ocean. Therefore, these novel capabilities of WEH are advantages over existing heaving cylinder. Although the floating energy harvester developed in the literature [20] contains some similar properties in design, there still exist two limitations compared to WEH developed in the study as: (1) The floating harvester is passive to ocean waves as it is unable to tune the frequency of ocean waves like WEH; (2) the floating harvester uses the bending piezoelectric effect d_{13}, which is smaller than the compressive piezoelectric effect d_{33} used in this work.

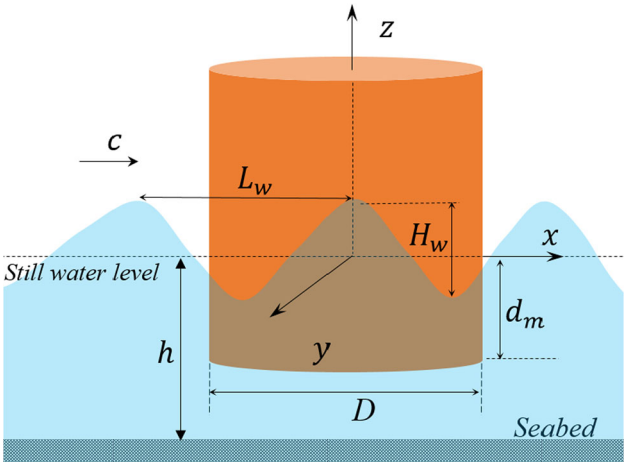

Fig. 1 Floating cylindrical structure on the ocean floor in xyz coordinate system

2 Design and Development of Mathematical Model for WEH

2.1 Ocean Wave–Structure Interaction

This section focuses on a practical analysis of the interaction between a cylindrical structure and ocean waves [21,22]. In reality, there are three main categories of ocean waves: linear wave sinusoidal profiles, nonlinear waves characterized by nonsymmetrical profiles, and random wave predictable in the frequency domain. These waves are induced by several activities, for example, winds, moving bodies (ship, boat…), earthquakes, gravitational force of moon and sun.

The wave–structure interaction in three dimensions is depicted in Fig. 1. The still water level is defined as the average water surface elevation at any moment. Notation h is water depth measured from the still water level; L_w, H_w and c are wave length, wave height, and phase velocity of waves, respectively; and d_m is the submerged portion height of the WEH that is defined as a distance between the WEH bottom and the still water level. It is noted that d_m can be adjusted by changing the WEH ballast material and WEH is sealed against seawater to protect its internal components during service. Under the impact of ocean waves in x-y-z coordinates, a rigid floating body experiences six coupled motions defined as surge: displacement along x-axis; sway: displacement along y axis; heave: displacement along z axis; roll: rotation about x-axis; pitch: rotation about y-axis; and yaw: rotation about z-axis.

This research considers the linear profile of waves profoundly studied in the literature [21]. Given the water depth, h, wave period, T, and gravitational acceleration, g =9.8 m/s^2, the wave length can be computed for deepwater waves [21]

Table 1 Properties of ocean waves, and material properties and dimensions of WEH

Dimensions		Properties	
$b_1 = b_3 = 0.025$ m	$s = 1.5$–2.4 mm	$m_1 = 0.4$ kg	$k_1 = 20000$ N/m
$b_2 = 0.05$ m	$s_m = 0.06$–0.1 m	$n = 10$–20	$\xi = 0.0017$
$a_1 = 0.1$ m	$h = 10$–30 m	$T = 6$–11s	$C_d = 0.47$–1.05
$a_2 = a_3 = 0.015$ m	$H_w = 1$–2 m	$E_l = 200$ GPa	$d_{33} = 6.5*10^{-10}$ C/N
$D = 0.8$–1 m	$L_h = 1$ m	$E_p = 70$ GPa	–
$c_v = 0.375$ (nF) for piezoelectric patch with geometry of 0.01 m, 0.01 m, 0.0001 m			

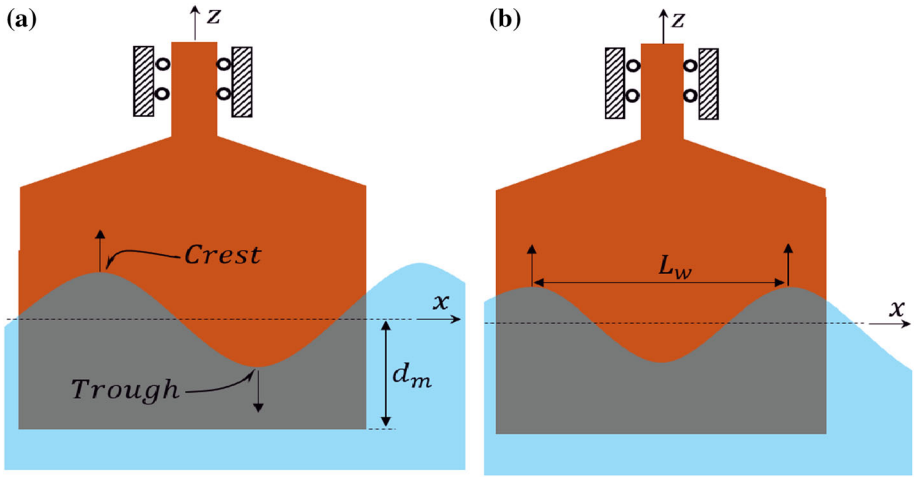

Fig. 2 Correlation between cylinder and wave crest for **a** no heave, **b** maximal heave

$$L_w = \frac{gT^2}{2\pi}\tanh\left(\frac{2\pi h}{L_w}\right) \approx \frac{gT^2}{2\pi} \tag{1}$$

Physically, the corresponding wave number, k_w, wave celerity, c, and the wave frequency, ω_w, can be provided as:

$$k_w = \frac{2\pi}{L_w}; \quad c = \frac{L_w}{T} \text{ and } \omega_w = k_w c = \frac{2\pi}{T} \tag{2}$$

The wave power occupied by the body for the deepwater condition in direction of wave propagation can be expressed as [21]

$$P_w = \frac{\rho g^2 H_w^2 TD}{32\pi} i \tag{3}$$

where notation D is the diameter of the cylindrical WEH; i stands for the direction of the wave propagation, i.e., x-direction as shown in Fig. 1; wave height H_w is selected in range of 1–2 m. In the study, it is noted that the wave height relates to water depth in reality, but mathematical relation between wave height and water depth is so far not established in existing studies. Therefore, the practical wave height and water depth are shown in Table 1.

The proposed design of the WEH is with respect to the heave motion; thus, motions such as roll, pitch, sway, surge, and pitching in x-y-z coordinate system shall be removed. To fulfill the design, firstly the WEH is fixed in directions other than z-direction shown in Fig. 2, and by this way, pitching and surging motions are deactivated. Besides, in order to achieve an optimal heave, the correlation between the WEH dimension and the wave length should be addressed before implementing the installation. Indeed, based on Fig. 2b, an extra either crest or trough on WEH produces a force only in z-direction leading to a pure heave, by the relationship, $D = j \cdot L_w/2$, $j = 1, 3, 5\ldots$. When the wave crest and trough apply to the WEH at the same time as shown in Fig. 2a equivalent with $D = j \cdot L_w$, $j = 1, 2, 3\ldots$, wave forces exerted on the structure are in an opposite direction. Thus, it induces only a pure pitching motion without any motions of heave or surge [23].

It is worthwhile noted that the design of the fixer in Fig. 2 is for a purpose showing the correlation between waves and structure. The real design of fixer for WEH is like that depicted in Fig. 3.

After these analyses, the dimensions of the WEH and ocean waves are selected appropriately in the modeling for a pure heave. Based on the Newton's second law, the wave–structure interaction equation of heaving motion for a floating cylindrical-shape body can be fully described following the work [21] as

$$(m_s + a_{am})\frac{d^2z}{dt^2} + b_{vz}\left(\frac{dz}{dt}\right)\left|\frac{dz}{dt}\right|^N + (b_{rz} + b_{pz})\frac{dz}{dt} + \left(\rho g \pi r^2 + Nk_s\right) z = F_{z0}\cos(\omega_w t + a_z) \tag{4}$$

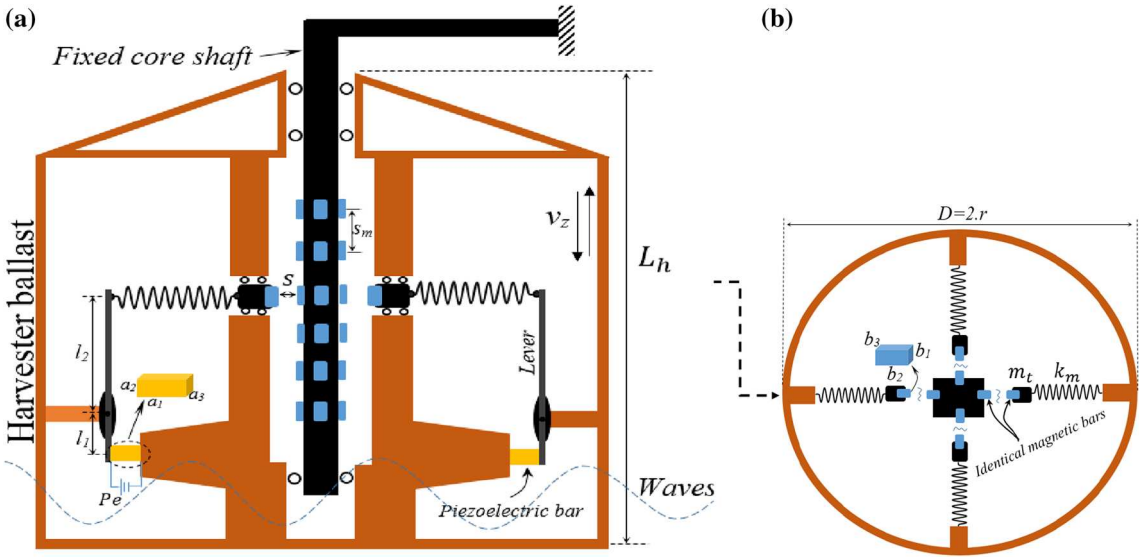

Fig. 3 Internal design of WEH; **a** side view; **b** cross-sectional view

where, m_s is the mass of the submerged part of the WEH that is equal to the mass of the displaced water and can be computed as

$$m_s = \rho_w d_m \pi r^2 \tag{5}$$

where r is the radius of cylindrical WEH, i.e., $D/2$.

a_{am} is the added mass that is the inertia applied to the WEH due to the presence of its body in a moving fluid or due to the motion of its body in a stationary fluid. The added mass is dependent on the frequency of ocean waves [24,25]. Since this work develops WEHs working in less varying frequencies, the added mass induced by interaction between cylinder with a circle cross section and ocean wave can be obtained as [21]

$$a_{am} = \pi \rho_w \frac{r}{2k_w^2} \frac{\cosh\left[k_w\left(h - d_m\right)\right]}{\cosh\left(k_w h\right)} H_1\left(2k_w r\right) \tag{6}$$

where ρ_w is the density of seawater (1030 kg/m^3) and $H_1(2k_w r)$ is the Struve function of one order derived as [26]

$$H_1\left(2k_w r\right) = \frac{2}{\pi}\left[\frac{(2k_w r)^2}{1^2 \cdot 3} - \frac{(2k_w r)^4}{1^2 \cdot 3^2 \cdot 5} + \frac{(2k_w r)^6}{1^2 \cdot 5^2 \cdot 7} \cdots\right] \tag{7}$$

b_{vz} and b_{rz} in Eq. (4) are the viscous and radiation damping coefficients, respectively. These are the results of the energy dissipation due to waves created by the converter heaving on the water surface. These waves take energy away from WEHs. For the WEH with cylinder profile in finite water depth in Fig. 1, the viscous damping and radiation coefficients can be estimated as [21]

$$b_{vz} \simeq \frac{\pi \rho_w C_d r^2}{2} \tag{8}$$

and

$$b_{rz} = \frac{\omega_w}{k_w} \rho_w \pi r^2 \frac{\cosh\left[k_w\left(h - d_m\right)\right]}{\cosh\left(k_w h\right)} \left[1 - \frac{J_1\left(2k_w r\right)}{k_w r}\right] \tag{9}$$

where C_d is drag coefficient, and it is equal to 0.47 for a circle cross section [27]. $J_1(2k_w r)$ is the first order of Bessel function of the first kind described as

$$J_1\left(2k_w r\right) = \sum_{j=0}^{\infty} \frac{(-1)^j}{j!\,(1+j)} \left(k_w r\right)^{1+2j} \tag{10}$$

b_{pz} in Eq. (4) is the power takeoff (POT) coefficient, which is an amount of ocean wave energy converted into the electricity by one WEH and the energy dissipation by the internal structure friction [21]. In this work, only the generated energy and the internal structure energy loss (e.g., viscous damping and internal structure friction of lever) are considered as the power takeoff. Other energy losses by rolling wheels are ignored in this study. By defining c_{pz} as a power takeoff coefficient of one generator, we have a relationship, $b_{pz} = 4c_{pz}$ as there are four mass-spring-damper systems in one WEH. The mathematical formulation of the coefficient c_{pz} will be characterized in the next subsection.

k_s in Eq. (4) is the spring constant of mooring lines, and N is the number of lines (mooring restoring force). In the design, there are no mooring lines, so $N = k_s = 0$.

F_{z0} in Eq. (4) is the amplitude of the wave-induced heaving force, which is computed as [21]

$$F_{z0} = \frac{\rho_w g H_w r L_w}{\pi}\left(e^{-\frac{2\pi d_m}{L_w}} + 1\right)\sin\left(\frac{2\pi r}{L_w}\right) \tag{11}$$

a_z in Eq. (4) is the phase angle between the wave and the force. Since the WEH is designed to be symmetric about planes x-y and y-z, a_z can be adopted as zero [21].

By taking into account the given values of $N = k_s = a_z = 0$, the steady solution form of Eq. (4) is characterized as

$$z = z_0 \cos\left(\omega_w t + a_z - \varepsilon_z\right) \tag{12}$$

where z_0 is the amplitude of the WEH heave motion and ε_z is the phase angle between the wave force and motion direction. The amplitude is thus obtained as

$$z_0 = \frac{\frac{F_{z0}}{(\rho_w g \pi r^2)}}{\left[\left(1 - \frac{\omega_w^2}{\left(\frac{\rho_w g \pi r^2}{m_s + a_{am}}\right)}\right)^2 + \left[\frac{\omega_w (b_{rz} + b_{vz} + b_{pz})}{\rho_w g \pi r^2}\right]^2\right]^{1/2}} \tag{13}$$

and

$$\varepsilon_z = \tan^{-1}\left[\frac{\frac{\omega_w^2 (b_{rz} + b_{vz} + b_{pz})}{\rho_w g \pi r^2}}{\left(1 - \frac{\omega_w^2}{\frac{\rho_w g \pi r^2}{m_s + a_{am}}}\right)}\right] \tag{14}$$

It can be seen from Eqs. (9)–(14) that the amplitude, damping coefficients, and angle are dependent on the ocean wave frequency. By substituting Eqs. (13) and (14) into Eq. (12), we obtain a full heaving motion equation of the WEH as follows:

$$z = \frac{\frac{F_{z0}}{(\rho_w g \pi r^2)}}{\left[\left(1 - \frac{\omega_w^2}{\frac{\rho_w g \pi r^2}{m_s + a_{am}}}\right)^2 + \left[\frac{\omega_w (b_{rz} + b_{vz} + b_{pz})}{\rho_w g \pi r^2}\right]^2\right]^{\frac{1}{2}}} \times \cos\left\{\omega_w t - tan^{-1}\left[\frac{\frac{\omega_w (b_{rz} + b_{vz} + b_{pz})}{\rho_w g \pi r^2}}{\left(1 - \frac{\omega_w^2}{\frac{\rho_w g \pi r^2}{m_s + a_{am}}}\right)}\right]\right\} \tag{15}$$

2.2 Root-Mean-Square of Generated Power from the Developed WEH

2.2.1 Excited Magnetic Force

The converter prototype comprises of a fixed core shaft and cylindrical case freely vibrating in z-direction shown in Fig. 3. The fixed core shaft is attached by rectangular magnetic bars with dimensions of the height, b_1, length b_2, and width, b_3. The distance between two adjacent magnetic bars is set as s_m. Assuming that the section of the moving shaft containing magnetic bars is long enough, the magnetic force always exists between the moving shaft and the cylindrical case. The similar impulsive magnetic force obtained by the relative motion between two magnetic bars is adopted for wave energy converter based on electromagnetic effect and was presented by NAREC center [28]. In this work, the cylindrical case consists of four mass-spring-lever-piezoelectric systems (MLPSs). The piezoelectric bar has a cubic shape, and its one end is firmly fixed to the body of WEH and another end is bonded to short lever arm as shown in Fig. 3. The positive and negative electrodes are in contact with two ends to collect electricity output. In reality, more mechanical components should be added to it such as sealer to keep piezoelectric bars from humidity and seawater, supporters to hold piezoelectric bar at one position during service, and so on. The piezoelectric bar with a length of a_1, a width of a_2, and a height of a_3 is made of the lead zirconate titanate (PZT4). The WEH can be fixed with a heavier and larger submerged floating object equipped with a special stabilization device [29] which helps the object to be more stable and allows the energy harvester to have a free heave relative to it during service. When the WEH heaves, it is subjected to an impact of ocean waves and the cylindrical case moves with respect to the fixed shaft that leads to the change of distance, s. Thus, the magnitude of the repelling magnetic force varies accordingly. In addition, when the distance, s_m, is shortened, the frequency of magnetic force is increased. By this way, the excitation frequency can be tuned by adjusting the distance, s_m, leading to an increase in the power output [7,12]. It is also noted that a higher excitation frequency could avoid a possible electric leakage of the converter [30]. Considering that for a complete circle of WEH, its travelled distance is $4z_0$ corresponding to time T, wherein z_0 is reciprocal amplitude of WEH characterized as Eq. (15).

Subsequently, the repelling magnetic force may be described as an absolute sinusoidal form

$$F_r(t) = \left| F_{r0} \sin\left\{\pi \cdot \frac{4\int_0^{\frac{T}{4}} \dot{z}\,dt}{T s_m}\right\}\right| \tag{16}$$

where F_{r0} is the amplitude of the repelling magnetic force. The present study focuses on energy harvesting from the regular waves. Based on the empirical study [31], when the minimal distance between two opposite magnetic bars is set as s, the repelling force amplitude F_{r0} between two magnetic bars can be calculated by:

$$F_{r0} = b_2 b_1^{4/3} B_r \left|B(s)\right| J(s), \tag{17}$$

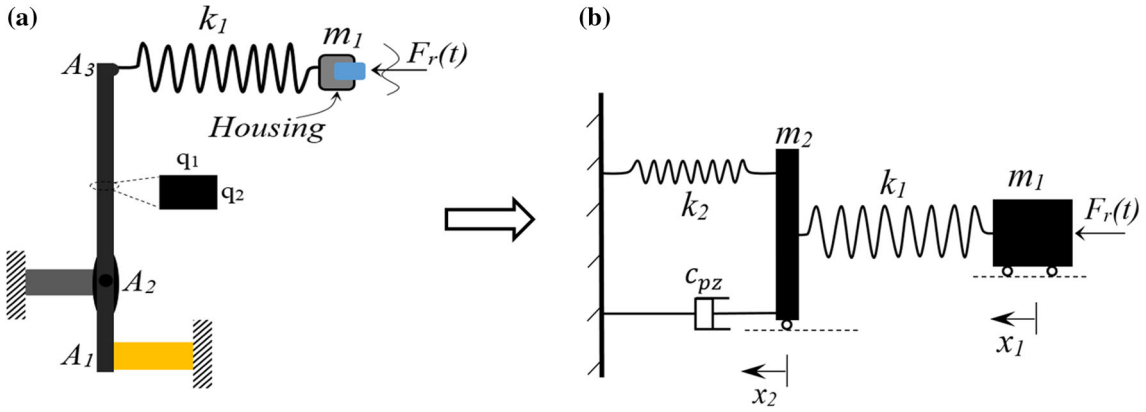

Fig. 4 Conversion of an MLPS into a two-degrees-of-freedom system. **a** MLPS, **b** two-degrees-of-freedom system

The magnetic bar is selected as neodymium iron boron, N5311 [32], having an equivalent magnetic residual flux density, Br. The material properties and dimensions of the components are provided in Table 1, unless otherwise noted. $B(s)$ and $J(s)$ are the magnetic flux density field and the decay function of repelling force between two magnetic faces, respectively. For a rectangular magnet, functions $B(s)$ and $J(s)$ can be obtained as [33]

$$B(s) = \frac{Br}{\pi}\left[\tan^{-1}\left(b_1 b_2 / \left\{2s\sqrt{4s^2 + b_1^2 + b_2^2}\right\}\right)\right] - \tan - 1b1b2/\{2b1 + s4b1 + s2 + b12 + b22\}, \tag{18}$$

and

$$J(s) = \left(1.749 + 1.145e^{(-s/s_0)}\right) \times 10^6 (\mathrm{NT}^{-2}\mathrm{m}^{-7/3}), \tag{19}$$

where s_0 is standardly selected to be 1 mm.

2.2.2 Generated Power

The MLPS comprises a mass-spring system and a lever fixed with a piezoelectric bar as shown in Fig. 4a. The mathematical model of the MLPS can be characterized by a two-degrees-of-freedom model [34] and is shown in Fig. 4b. Based on Fig. 4a, MLPS contains a moving mass, m_1, and a connecting spring with spring stiffness, k_1. Vibrational mass is considered as a sum of the housing mass and magnetic bar mass.

In Fig. 4, the lever made of a steel bar with a long moment arm, l_2, and short moment arm, l_1, is able to freely rotate around point, A_2, and its equivalent lever moment ratio is defined as $n = l_2/l_1$. $l_1 = 0.02$m is chosen throughout the research. Both tips of the lever are connected with the mass-spring system and piezoelectric transducer at points A_3 and A_1, respectively, depicted in Fig. 4a. The piezoelectric bar is fixed on the WEH frame. The parameters of the mass-spring-damper system can be derived from material properties and dimensions of the equivalent cantilever beam below [35]:

$$\begin{cases} k_1 = E_1 q_1^3 q_2 / \left(4 l_1^3 n^3\right) \\ m_2 = \rho_1 A_1 l_1 n) \\ c_1 = 2\xi\sqrt{k_1 m_2} \end{cases} \tag{20}$$

where E_l, ρ_l, A_l, m_2, and ξ are Young's modulus, material density, cross-section area, equivalent mass of lever, and damping ratio of lever arms, respectively. k_1 is the spring constant corresponding to the elastic deflection of beam tip, A_1. c_1 is the mechanical damping coefficient of the beam that is induced by the internal structural damping force [36] and the friction between the cantilever beam and the viscous air in vibration process. The spring stiffness of the piezoelectric bar in the direction of pulling force is $k_p = E_p a_2^2/(a_1 n^2)$, which also contributes to the stiffness of lever-piezoelectricity device. Hence, the total spring constant, k_2, of the lever-piezoelectricity device now can be obtained as $k_2 = k_1 k_p / \left(k_p + k_1\right)$. The lever cross section is designed as a rectangular shape with a height and width of q_1 and q_2, respectively, as shown in Fig. 4a. Their values are firmly selected as $q_1 = 0.03$ m and $q_2 = 0.015$ m, unless otherwise noted. The total damping coefficient, c_{pz}, of MLPS includes a lever damping coefficient, c_l, and electric damping coefficient, c_e, from a closed electric circuit [37], which connects directly to the piezoelectric transducer. Thus, the total damping coefficient of MLPS is $c_{pz} = c_e + c_1$.

Where the electrical damping coefficient, c_e, can be derived as [38]:

$$c_e = n^2 d_{33}^2 k_2^2 / (\pi^2 c_a f) \tag{21}$$

In Eq. (21), d_{33} is the piezoelectric constant in the polling direction; c_a is the electric capacity of the piezoelectric bar; f is the first natural vibration frequency of the spring-mass

system shown in Fig. 4b, and it can be determined by using the numerical solution [39]. After the specific descriptions of MLPS components are presented, the generated output power of the WEH is calculated hereafter. Based on the Newton's second law, the oscillating equation of the MLPS shown in Fig. 4 can be written:

$$\begin{cases} \dot{z} = f_{\dot{z}}(\omega_{\mathrm{w}}, b_{\mathrm{rz}}, b_{\mathrm{vz}}, b_{\mathrm{pz}}, m_{\mathrm{s}}, a_{\mathrm{am}}, t) \\ \ddot{x}_1 = \frac{k_1(x_2-x_1)}{m_1} + \frac{\left|F_{\mathrm{r0}} \sin\left\{4\pi \cdot \int_0^{\frac{T}{4}} \dot{z}\mathrm{d}t \cdot t/(T.s_{\mathrm{m}})\right\}\right|}{m_1} \\ \ddot{x}_2 = \frac{k_1(x_1-x_2)}{m_2} - \frac{k_2 x_2}{m_2} - \frac{c_{\mathrm{pz}}\dot{x}_2}{m_2} \end{cases} \tag{22}$$

where notation $f_{\dot{z}}$ is a function, which is obtained from a derivative of Eq. (15) with respect to t.

The Runge–Kutta method is adopted to solve Eq. (22). To do so, the transformation of second-order differential equation into first-order one is initiated by:

$$\begin{cases} \dot{x}_1 = v_1 \\ \dot{x}_2 = v_2 \end{cases} \Longrightarrow \begin{cases} \dot{v}_1 = \ddot{x}_1 \\ \dot{v}_2 = \ddot{x}_2 \end{cases} \tag{23}$$

where v_1 and v_2 are the velocities of the moving mass and tip, B, of the lever, respectively. In this work, we define a notation, v_z, as the average vertical speed of harvester ballast, which can be evaluated as $v_z = 4\int_0^{\frac{T}{4}} \frac{\dot{z}\mathrm{d}t}{T} = 4Z_0/T$ Subsequently, from Eqs. (22) and (23), a system of the first-order differential equations is written as

$$\begin{cases} \dot{v}_1 = f_1(t, x_1, x_2, v_z) \\ \dot{v}_2 = f_2(x_1, x_2, v_2) \\ \dot{x}_1 = f_3(v_1) \\ \dot{x}_2 = f_4(v_2) \end{cases} \tag{24}$$

Iteration method with the time step, $\Delta t < 10^{-4}$ s, is developed to solve Eq. (24) as

$$\begin{cases} t_{i+1} = t_i + \Delta t \\ g_1(t_i) = f_1(t_i, x_1(t_i), x_2(t_i), v_z(t_i)) \\ g_2(t_i) = f_2(t_i, x_1(t_i), x_2(t_i)) \\ v_1(t_{i+1}) = v_1(t_i) + g_1(t_i) \cdot \Delta t \qquad i = 0, 1, 2, \ldots, \infty. \\ v_2(t_{i+1}) = v_2(t_i) + g_2(t_i) \cdot \Delta t \\ x_1(t_{i+1}) = x_1(t_i) + f_3(v_1(t_{i+1})) \cdot \Delta t \\ x_2(t_{i+1}) = x_2(t_i) + f_4(v_2(t_{i+1})) \cdot \Delta t \end{cases} \tag{25}$$

The zero values of initial condition can be used as $i = 0$, $t_0 = 0$, $x_1(t_0) = 0$, $x_2(t_0) = 0$, $v_1(t_0) = 0$, and $v_2(t_0) = 0$ for the solution of Eq. (25).

Consequently, the electric charge, voltage, and current produced by each MLPS at time t_i are:

$$\begin{cases} Q(t_i) = d_{33} n k_2 X_2(t_i) \\ V(t_i) = d_{33} n k_2 X_2(t_i)/C_a, \\ I(t_i) = d_{33} n k_2 v_2(t_i) \end{cases} \tag{26}$$

The electric capacity of the piezoelectric material can be computed as [40]

$$c_a = \xi_a c_v a_2 a_3 / a_1 \tag{27}$$

The value of c_v is provided in Table 1, and notation ξ_a is piezoelectric material difference correction between this work and work [40] selected as $\xi_a = 0.89$. The electric power output of one MLPS at time t_i from the piezoelectric effect now can be obtained as:

$$P_{e1}(t_i) = d_{33}^2 n^2 k_2^2 x_2(t_i)\, v_2(t_i)/c_a. \tag{28}$$

When the WEH works for a time duration τ, total RMS of the generated electric power of four MLPSs from time 0 to τ can be computed by:

$$P_{\mathrm{e}} = 4\sqrt{\frac{1}{\tau}\int_0^{\tau} P_{e1}^2(t)\,\mathrm{d}t} \tag{29}$$

When τ is divided into μ small time intervals, the discrete expression of Eq. (29) can be rewritten as:

$$P_{\mathrm{e}} = 4\sqrt{\frac{1}{\mu}\sum_{i=1}^{\mu} P_{e1}^2(t_i)} \tag{30}$$

The conversion efficiency of WEH with four MLPSs now can be written as

$$f_{\mathrm{e}} = \frac{P_{\mathrm{e}}}{P_{\mathrm{w}}} 100\% \tag{31}$$

The data for computing the power output are provided in Table 1 unless otherwise noted. It is noted that some data are indicated in a specific range for the purpose of the investigation of the effects on the power output and energy conversion efficiency of the proposed WEH.

3 Results and Discussion

In order to obtain an optimal design of the WEH for a high power output, the effects of the converter components' material properties and dimension by the developed mathematical model are investigated.

To ascertain the soundness of the developed WEH and its modeling, the oscillation of the vibrational mass is calculated and illustrated in Fig. 5 with the parameters of n = 15, C_{d} = 0.47, d_{m} = 0.25 m, T = 8 s, D = 0.8 m, H_{w} = 1.5 m,

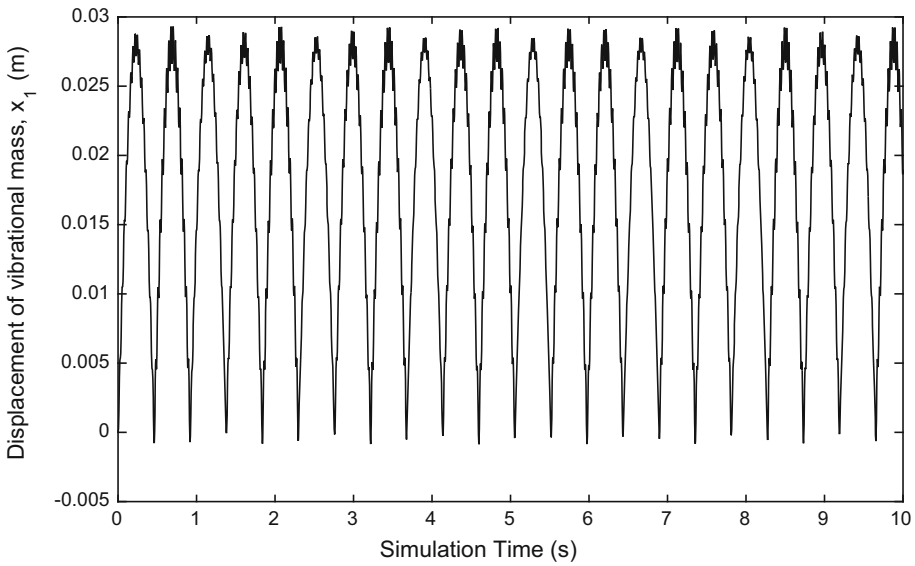

Fig. 5 Oscillation of vibrational mass

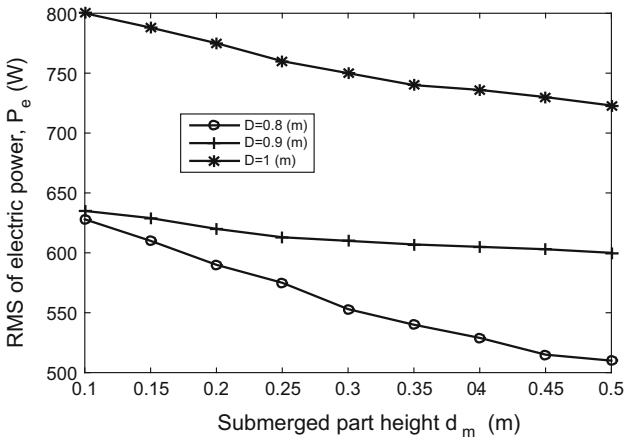

Fig. 6 Influence of submerged portion height on RMS of the power with different WEH diameter

h = 20 m, s = 0.002 m, and s_m = 0.06 m. It is observed from Fig. 5 that the oscillating amplitude and period of the vibrational mass are around 0.03 m and 0.5 s, respectively. This period is 16 times smaller than that of ocean waves meaning that the frequency of MLPS is magnified 16 times with respect to the low-frequency ocean waves (equivalent to T = 8 s).

Investigations on the effect of properties and dimensions of ocean waves and converter's components on the generated electric power are provided as follows. The influence of the submerged portion height of the WEH on the power output at different diameters, D = 1 m, 1.5 m and 2 m, is shown in Fig. 6. Wherein other parameters are n = 15, C_d = 0.47, T =8 s, H_w = 1.5 m, h = 20 m, s = 0.002 m, and s_m = 0.06 m. Generally, based on the figure, the generated power nonlinearly decreases with a rise of submerged portion height. When the submerged height, d_m, increases from 0.1 m to 0.5 m, the electric power goes down from 800 W to 720 W at D = 1 m. The power can reach up to 750 W at a submerged portion height and a wave height of d_m = 0.3 m and D = 1 m, respectively. In order to have a desired value of the submerged height of WEH, we can manually adjust it by changing the material of converter ballast [21]. The observation in the figure can be explained: Based on Eqs. (8) and (9), an increase in the submerged height leads to a rise of the value of the wave viscous and radiation damping. In addition, Fig. 6 shows a rise of power output with an increase in the WEH diameter since the diameter larger size leads to more energy from ocean waves interacting on the converter. Specifically, at d_m = 0.1 m, the power at D = 0.8 m is nearly equal to that of D = 0.9 m. This abnormal results are due to the reason that WEH reaches a near-resonance condition at d_m = 0.1 m and D =0.8 m leading to higher power output. Such phenomena will be investigated afterward.

Figure 7 shows the influence of distance between two adjacent magnetic bars and distance between two opposite magnetic bars on RMS of electric power. Other parameters are n = 15, C_d = 0.47, T =8 s, H_w = 1.5 m, h = 20 m, d_m = 0.25 m, and D = 0.8 m. The figure demonstrates a sudden rise of the power output up to 1100 W at s = 1.5 mm and s_m =0.07 m. This finding can be interpreted by the fact that the change of the distance s_m results in a variation of excitation frequency. At a proper value of s_m, the excitation frequency matches the natural frequency of MLPS system leading to an occurrence of resonance. In this case, at s =0.0015 m, s_m = 0.07 m, and given inputs, a near-resonance condition occurs; hence, the power output is outstandingly high. The finding is important as we can track and set the value of distance between two adjacent magnetic bars, s_m, to obtain the resonance for higher generated power. Based on the mathematical result, the damping level for resonance condition

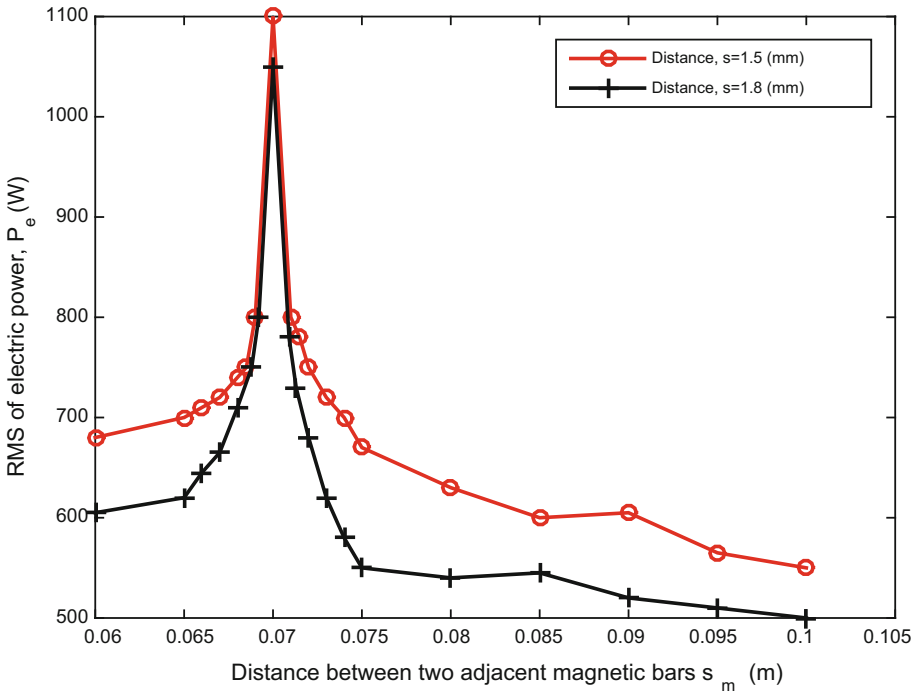

Fig. 7 Influence of distance between two adjacent magnetic bars and distance between two opposite magnetic bars on RMS of electric power

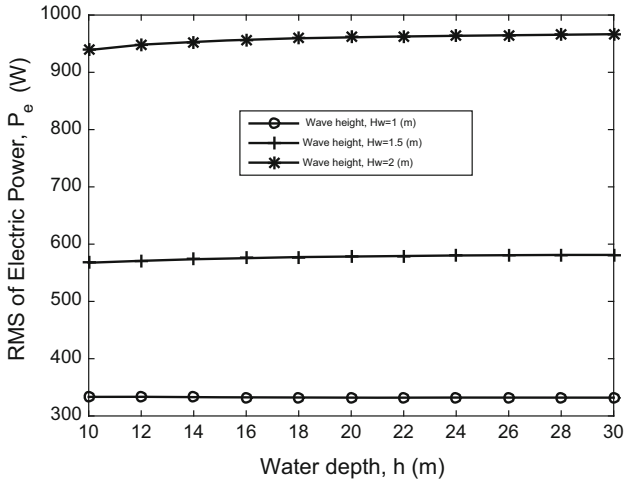

Fig. 8 Influence of the water depth and wave height on RMS of the power

occurrence is around b_{pz} = 9000 (Ns/m). In addition, Fig. 7 reveals a decrement in RMS of power with an increase in the distance s_m for off-resonant regions. The finding is obvious when the distance $s_m$is longer, and the excitation frequency is lower.

The influence of the water depth and wave height on RMS of the power is demonstrated in Fig. 8 with parameters being n = 15, C_d = 0.47, T =8 s, s =0.002m, s_m = 0.06 m, d_m = 0.25 m, and D =0.8 m. It is observed from the figure that the water depth has little effect on the electric generation of the WEH. It is interpreted that based on the iterative solution of Eq. (1), when water depth varies, the wavelength output L_w has a little increment. As a result, giving that wave velocity is constant, the wave period T and wave power P_w will has a small increment based on Eqs. (2) and (3) leading to small change in power output. However, a rise of wave height leads to an increase in the power output. It is indicated in Fig. 8 that the power output is up to 950 W at h = 20 m, H_w = 2 m. It can be explained that based on Eq. (3), the wave power is proportional to square power of wave height. Hence, a higher wave power is achieved on the WEH leading to higher power output supposing that its energy conversion is unchanged for these conditions.

Given that ocean depth h is unchanged, from Eqs. (1), (2), and (9), the wave period T is the only influential component of hydrodynamic radiation damping coefficient, b_{rz}. Hence, understanding the effect of T on power output will help us identify the influence of b_{rz} on power output. It is noted from Fig. 8 that the power output is almost unchanged with the variation of h. Thus, it is difficult to understand the effect of b_{rz} on electric power through h. Fig. 9 shows the effect of wave period on the power output with H_w = 1.5 m, n = 15, C_d = 0.47, s = 0.002 m, s_m = 0.06 m, d_m = 0.25 m, and D = 0.8 m. The figure shows a nonlinear reduction of the electric power with respect to a rise of T. It is seen that when wave period increases from 6 s to 11 s, the electric power decreases from 730 W to 460 W, respectively. It can be interpreted that based on Eqs. (1), (2), and (9), increasing the wave period causes a rise in hydrodynamic radiation damping coefficient value b_{rz}. In addition, a lower wave period leads to a higher frequency of excited force (characterized

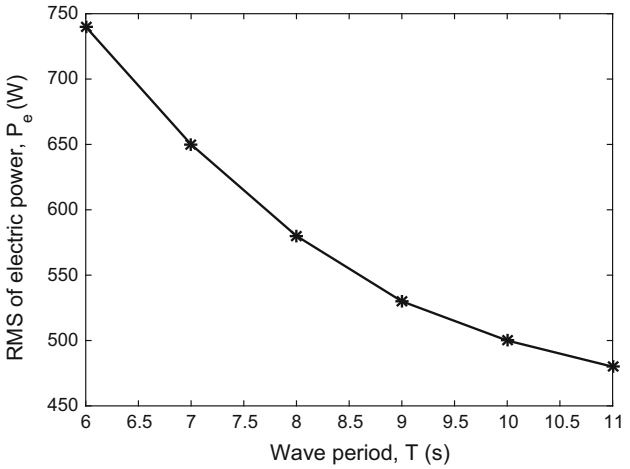

Fig. 9 Effect of wave period on the power output

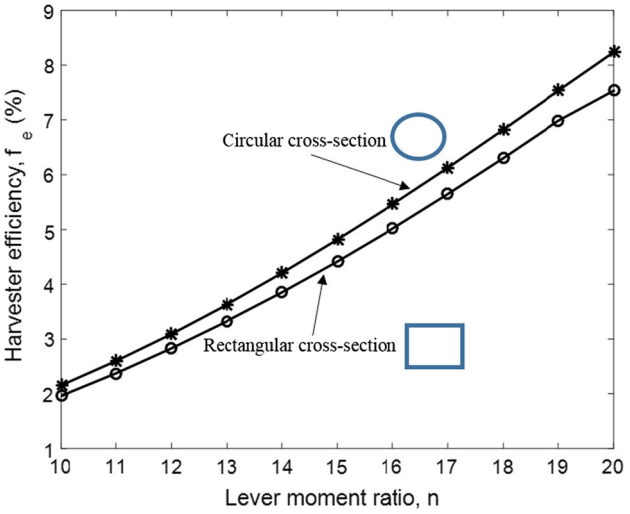

Fig. 10 Effect of WEH cross section and lever moment ratio on the energy conversion efficiency

by Eq. (17)) applied to the piezoelectric transducer, which results in a higher efficiency of piezoelectric transducer.

Understanding the energy conversion efficiency of the proposed WEH is also important to know the effectiveness of design. The energy conversion efficiency of WEH as the percentage of generated power per wave power of an area occupied by the harvester based on Eq. (31) versus the change of lever moment ratio with different cross-section shapes of converter is illustrated in Fig. 10. Other parameters are provided in Table 1 and are set as $T = 8$ s, $s = 0.002\ m, s_m = 0.06$ m, $d_m = 0.25$ m, $h = 20$ m, $H_w = 1.5$ m, and $D = 0.8$ m. It can be seen from the figure that the power output increases with a rise of lever moment ratio. It is due to the fact that the force applied to the piezoelectric transducer is magnified with a rise of the lever moment ratio [41]. In addition, the figure reveals an important result that the WEH with a cylindrical shape results

Table 2 Comparison of power output between the proposed WEH and OPT PB3

	Proposed WEH	OPT PB3
Transduction type	Piezoelectricity	Electromagnetism
Total weight (kg)	50	10,208
Floating diameter (m)	0.8	2.7
Floating height (m)	1	3.5
RMS of generated power (W)	750	350

in a higher energy conversion efficiency than that of prism shape with rectangular cross section. At a lever moment ratio $n = 15$, the WEH with a circular cross section has an energy conversion efficiency around 0.4 % higher than that with rectangular cross section. One of the reasons may be due to that the drag coefficient of rectangular cross section ($C_d = 1.05$) is higher than that of circular cross section ($C_d = 0.47$). And based on Eq. (8), the wave viscous damping during the wave–object interaction of the WEH with a rectangular cross section is higher than that of a circular cross section. From this observation, we suggest to consider an WEH with a circular cross section.

Table 2 shows a comparison of average power output between the proposed WEH and OPT PB3 [42]. The data used for the comparison are selected as $n = 15$, $C_d = 0.47$, $T = 8$ s, $H_w = 1.5$ m, $h = 20$ m, $D = 1$ m, $d_m = 0.25$ m, $s = 0.002$ m, and $s_m = 0.06$ m. Due to the heave motion, OPT PB3 converts the linear motion into a rotary motion that drives an electric generator to produce electricity based on the electromagnetic effect. The system is kept working stably on ocean floor by a mooring device. It is noted that in Table 2, the weight of OPT PB3 consists of the total weights of equipment plus auxiliary devices including the battery. However, the weight of WEH only includes the primary energy conversation units, but does not include the auxiliary devices such as battery. Owing to the fact, in the design of WEH, auxiliary devices are located on the fixer of WEH. Table 2 shows that the proposed WEH can generate 750 W which is approximately two times higher than that of OPT PB3, i.e., 350 W, although the diameter and floating height of proposed WEH are nearly half of OPT PB3. It is noted that power value of 750 W is obtained under off-resonance condition. There are two reasons for the observations. Firstly, the proposed WEH uses piezoelectric transducer whose energy density is three times higher than that of electromagnetic transducer used by OPT PB3 [7]. Secondly, the proposed converter is able to magnify low-frequency ocean waves to a high excitation frequency in order to harness higher power output. Such capability is not utilized by OPT PB3. In addition, another advantage of the WEH over the OPT PB3 is that its design is simple and utilizes fewer components, but only magnetic bars, mass-spring system, lever, piezoelectric bars. The WEH has a small size,

which saves the space occupied by the WEH on ocean floor. As a result, these advantages can facilitate its installation, maintenance, and repair.

4 Conclusion

The development of a novel piezoelectric WEH is presented to harvest high energy from low-frequency ocean waves. The presented WEH is composed of a cylindrical case moving with respect to the fixed core shaft attached to identical magnetic bars. The cylindrical case contains four MLPSs arranged symmetrically each other via the fixed shaft. By this innovative design, the advantages of proposed WEH are (i) The ocean waves with a lower frequency are converted into a force of a higher excitation frequency; (ii) off-resonance and resonance conditions are observed with the proposed WEH when it interacts with ocean waves; (iii) the developed WEH is able to increase the power output by adjusting the distances, size, and material properties of its internal component without increasing the WEH's physical size; (iv) the WEH design is simple, economic, efficient, and well adaptive to ocean harsh environment. Indeed, our findings indicate that the power output increases with rises of the ocean wave height and the WEH diameter, and decreases in the distance between two adjacent magnetic bars on the fixed shaft, distance between two opposite magnetic bars, and WEH's submerged portion height. Furthermore, the water depth shows little effect on the power output. The WEH with a circular cross section has higher energy conversion efficiency than that with a rectangular cross section. A power of 750 W is realized with the WEH height and diameter, ocean wave height, and wave period being 1 m, 1 m, 1.5 m, and 8 s, respectively. A comparison with another electromagnetic converter, OPT PB3, which also uses the heave to produce electricity, is carried out. The power output of the proposed WEH is two times higher than that of OPT PB3, and even its dimension is two times smaller than that of OPT PB3.

Acknowledgements This research did not receive any specific grant from funding agencies in the public, commercial, or not-for-profit sectors.

References

1. Khaligh, A.; Onar, O.C.: Energy Harvesting: Solar, Wind, and Ocean Energy Conversion Systems (Energy, Power Electronics, and Machines), p. 1. Hardcover, Boca Raton (2009)
2. Falnes, J.: A review of wave-energy extraction. Mar. Struct. **20**, 185–201 (2007)
3. Zhang, Y.L.; Lin, Z.: Advances in technology of ocean wave energy converters using piezoelectric materials. J. Hydroelectr. Eng. **5**, 324–331 (2011)
4. Anton, S.R.; Sodano, H.A.: A review of power harvesting using piezoelectric materials 2003–2006. Smart. Mater. Struct. **16**, 21–27 (2007)
5. http://acore.org/wp-content/uploads/2012/01. Accessed 9 Apr 2018
6. Sravanthi, C; James, M.C.: A Survey of Energy Harvesting Sources for Embedded Systems. IEEE (2008)
7. Williams, C.B.; Yates, R.B.: Analysis of a micro-electric generator for microsystems. Sens. Actuators A **52**, 8–11 (1996)
8. Priya, S.: Advances in energy harvesting using low profile piezoelectric transducers. J. Electroceram. **19**, 165–182 (2007)
9. http://www.piezo.com/tech3faq.html. Accessed 9 May 2018
10. Gu, L.; Livermore, C.: Passive self-tuning energy harvester for extracting energy from rotational motion. Appl. Phys. Lett. **97**, 04–09 (2016)
11. Viet, N.V.; Wu, N.; Wang, Q.A.: review on energy harvesting from ocean waves by piezoelectric technology. J. Mod. Mech. Mater. **4**, 161–171 (2017)
12. Murray, R.; Rastegar, J.: Novel two-stage piezoelectric-based ocean wave energy harvesters for moored or unmoored buoys. Act. Passive Smart Struct. Integr. Syst. SPIE **7288**, 1117–1129 (2009)
13. Miller, L.M; Wright, P.K; Ho, C.C; Evans, J.W; Shafer, P.C; Ramesh, R.: Integration of a low frequency, tunable MEMS piezoelectric energy harvester and a thick film micro capacitor as a power supply system for wireless sensor nodes in IEEE, ECCE, 27–34 (2009)
14. Zhou, S.; Cao, J.; Erturk, A.; Lin, J.: Enhanced broadband piezoelectric energy harvesting using rotatable magnets. Appl. Phys. Lett. **102**, 01–05 (2013)
15. Erturk, A.; Hoffmann, J.; Inman, D.J.: A piezomagnetoelastic structure for broadband vibration energy harvesting. Appl. Phys. Lett. **94**, 02–06 (2009)
16. Zhou, S.; Cao, J.; Inman, D.J.; Liu, S.; Wang, W.; Lin, J.: Impact-induced high-energy orbits of nonlinear energy harvesters. Appl. Phys. Lett. **106**, 01–06 (2015)
17. Xie, X.D.; Wang, Q.; Wu, N.: A ring piezoelectric energy harvester excited by magnetic forces. Int. J. Eng. Sci. **77**, 71–78 (2014)
18. Viet, N.V.; Al-Qutayri, M.; Liew, K.M.; Wang, Q.: An octo-generator for energy harvesting based on the piezoelectric effect. Appl. Ocean Res. **64**, 128–134 (2017)
19. Viet, N.V.; Wang, Q.; Carpinteri, A.: Development of an ocean wave energy harvester with a built-in frequency conversion function. Int. J. Energy. Res. **42**, 684–695 (2017)
20. Wu, N; Wang, Q; Xie, X.: Ocean wave energy harvesting with a piezoelectric coupled buoy. US Patent 9,726,143, 08/August (2017)
21. McCormick, M.: Ocean Engineering Mechanics With Applications. Cambridge University Press, New York (2009)
22. McCormick, M.: Ocean Wave Energy Conversion. Dover Publications, Mineola, NY (2007)
23. Rafael, E.V.; Carl, D.C.; Julio, C.C.: Analysis of a planar tensegrity mechanism for ocean wave energy harvesting. J. Mech. Robot. **6**, 31015–31021 (2014)
24. Kristiansen, E; Egeland, O.: Frequency dependent added mass in models for controller design for wave motion ship damping. MCMC'03, Girona, Spain 17–19 (2003)
25. Taghipour, R.; Perez, T.; Moan, T.: Hybrid frequency-time domain models for dynamic response analysis of marine structures. Ocean Eng. **35**(7), 685–705 (2008)
26. Abramowitz, M.; Stegun, I.A.: Handbook of Mathematical Functions, Dover Publications. New York. Originally published by the U. S. Printing Office, Washington, DC (1965)
27. https://en.wikipedia.org/wiki/Drag_coefficient. Accessed 9 Apr 2018
28. Spooner, E.; Grimwade, J.: Snapper^{TM}: an efficient and compact direct electric power take-off device for wave energy converters.

In: Proceedings of the World Maritime Technology Conference, 6–10 March, London, UK (2006)
29. John, S.W.M; Adams, D.: Gyroscopic roll stabilizer for boats. US10454905, 04/June (2003)
30. http://www.piezo.com/tech3faq.html. Accessed 5 Mar 2018
31. www.kjmagnetics.com/calculator.asp. Accessed 16 Mar 2018
32. http://www.intemag.com/magnetic_properties.html#neodymium_props. Accessed 9 May 2018
33. Al-Ashtari, W.; Hunstig, M.; Hemsel, T.; Sextro, W.: Frequency tuning of piezoelectric energy harvesters by magnetic force. Smart Mater. Struct. **21**, 19–24 (2012)
34. Viet, N.V.; Xie, X.D.; Liew, K.M.; Banthia, N.; Wang, Q.: Energy harvesting from ocean waves by a floating energy harvester. Energy **112**, 1219–1226 (2016)
35. Blevins, R.D.: Formulas for Natural Frequency and Mode Shape. Van Nostrand Reinhold, New York (1979)
36. Woodhouse, J.: Linear damping models for structural vibration. J. Sound. Vib. **215**(3), 547–69 (1998)
37. Mitcheson, P.D.; Yeatman, E.M.; Rao, G.K.; Holmes, A.S.; Green, T.C.: Energy harvesting from human and machine motion for wireless electronic devices. IEEE **96**, 1455–1458 (2008)
38. Xie, X.D.; Wang, Q.: Energy harvesting from a vehicle suspension system. Energy **86**, 385–92 (2015)
39. Ravi, T.T.; Krishna, C.T.: Computation of natural frequencies of multi degree of freedom system. Int. J. Eng. Res. Technol. **10**, 2278–2281 (2012)
40. Wu, N.; Wang, Q.; Xie, X.D.: Wind energy harvesting with a piezoelectric harvester. Smart Mater. Struct. **22**, 23–28 (2013)
41. Tao, J.X.; Viet, N.V.; Carpinteri, A.; Wang, Q.: Energy harvesting from wind by a piezoelectric harvester. Eng. Struct. **133**, 74–80 (2017)
42. http://www.oceanpowertechnologies.com/pb3/. Accessed 19 Apr 2018